14th International Symposium on Turbulence and Shear Flow Phenomena (TSFP14)
Heidelberg, Germany, July 28–31, 2026

DOMINANT VORTICITY/STRAIN CANCELLATIONS IN THE NONLINEAR PRESSURE–POISSON SOURCE OF TURBULENT CHANNEL FLOW

J. M. O. Massey
Center for Turbulence Research
Stanford University
Stanford, CA 94305, USA
masseyj@stanford.edu

J. C. Klewicki
Department of Mechanical Engineering
University of Melbourne
Melbourne, VIC 3010, Australia
klewicki@unimelb.edu.au

B. J. McKeon
Center for Turbulence Research
Stanford University
Stanford, CA 94305, USA
bjmckeon@stanford.edu

ABSTRACT

Wall-pressure variance in canonical turbulent wall-bounded flows grows approximately logarithmically with friction Reynolds number, and recent work has linked that growth primarily to the nonlinear source term in the pressure Poisson equation. Here we ask which exact decomposition of that source best exposes the wall-relevant dynamics. Using source-density attribution in a turbulent channel direct numerical simulation at friction Reynolds number about 550, we compare the standard gradient-product decomposition with the exact vorticity/strain decomposition. The gradient-product view suggests that two mixed-derivative terms dominate the wall-relevant source, while a third appears weak. The vorticity/strain view shows instead that this apparently weak contribution is the residual of one of the strongest near-wall cancellations. More broadly, the peak is the positive remainder of three dominant cancellations between the three vorticity components and their companion shear-strain terms, while the diagonal strain terms provide only modest corrections. These results identify the balances that reduced measurements and models must preserve to capture wall-pressure generation, and show that the vorticity/strain decomposition provides the clearer mechanistic description.

MOTIVATION AND OBJECTIVE

Wall-pressure fluctuations in turbulent wall-bounded flows underpin noise, structural fatigue and flow–structure coupling. A robust empirical observation is that the inner-scaled wall-pressure variance increases logarithmically with friction Reynolds number,

$$\langle p^{+2} \rangle = B_L + A \ln \delta^+, \qquad (1)$$

where, in this scaling discussion, p denotes the wall pressure, $p^+ = p/(\rho u_\tau^2) = p/\tau_w$, and $\delta^+ \equiv \delta u_\tau/\nu$ (with $\delta = h$, the channel half-height, for channel flow); u_τ is the friction velocity, τ_w the wall shear stress, ρ the fluid density, ν the kinematic viscosity, and A and B_L are empirical constants (Klewicki *et al.*, 2008; Fritsch *et al.*, 2020; Dacome *et al.*, 2025). Recent DNS-based work has shown that the logarithmic term in (1) is linked primarily to the nonlinear pressure source, while the linear source retains an approximately inner-scaled contribution under viscous normalisation (Massey *et al.*, 2025).

In incompressible turbulent flow, pressure is obtained from a Poisson equation. The linear (rapid) source couples the mean shear to the fluctuating velocity field; the nonlinear (slow) source comes from quadratic velocity–velocity interactions; and the viscous (Stokes) contribution enters through the wall boundary condition. The important practical point is that the wall pressure is not determined by the source at the wall alone. Rather, every wall-normal source sheet contributes through an elliptic Green's mapping. Existing source-attribution studies therefore show two complementary facts: the dominant inner-scaled contribution comes from the near-wall/buffer region, while long wall-parallel wavelengths can sample farther from the wall through the Green's kernel (Kim, 1989; Anantharamu & Mahesh, 2020; Massey *et al.*, 2025).

Recent work suggests that the inertial-layer contribution to wall pressure is concentrated near interfaces between uniform-momentum zones, where thin, intense sheets of spanwise vorticity provide compact carriers of the nonlinear source (Bautista *et al.*, 2019; Massey *et al.*, 2025; Deshpande *et al.*, 2025). Figure 1, reproduced from Massey *et al.* (2025), summarises that structural picture. The present paper does not attempt to re-establish it. Instead, it addresses the algebraic question that precedes any reduced model built around it: which exact decomposition of Q makes the wall-relevant balance most transparent?

The objective is therefore one of elucidating the underlying mechanisms rather than asymptotic behaviour. Using a single turbulent channel DNS at $\delta^+ \approx 550$, we compare the standard gradient-product form of Q with the exact vorticity/strain form through direct wall-pressure source attribution. The key result is that the gradient-product terms are themselves residuals, whereas the vorticity/strain form isolates the three large cancellations whose positive remainder produces the peak. Thus, any reduced surrogate must preserve that remainder.

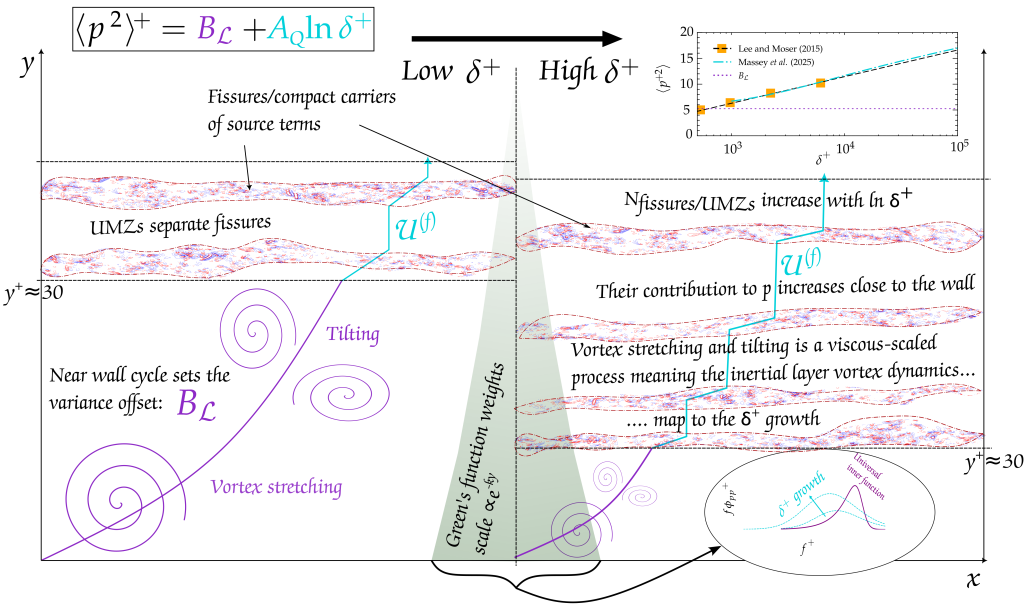

Figure 1. Reproduced from Massey *et al.* (2025). Schematic of the physical process proposed to yield the $\ln \delta^+$ growth of $\langle p^{+2}\rangle$. Vortex stretching/tilting produces thin, sheetlike fissures that carry Poisson sources compactly across the inertial layer and imprint at the wall through an elliptic Green's mapping that favours low wall-parallel wavenumbers. Inset reproduced from Massey *et al.* (2026).

NONLINEAR PRESSURE–POISSON SOURCE AND ITS TWO EXACT FORMS

We use the decomposition of Mansour *et al.* (1988) and Kim (1989). Adopting the coordinate system $x_i \in \{x, y, z\}$, where x is streamwise, y is wall normal, and z is spanwise, and using the Einstein summation convention, the fluctuating pressure satisfies

$$\begin{aligned} \partial_i \partial_i \pi &= -2\,\frac{\mathrm{d}U}{\mathrm{d}y}\,\partial_x v + Q, \\ Q \equiv -\partial_j \partial_k \left(u_j u_k\right) &= -\partial_j \left[(u\cdot\nabla) u_j\right] = -\partial_j u_k\,\partial_k u_j, \end{aligned} \tag{2}$$

where π denotes the fluctuating kinematic pressure, and no-slip is enforced through the Neumann condition

$$\partial_y \pi\big|_w = \nu\,\partial_y \partial_y v\big|_w. \tag{3}$$

Accordingly, the full-field decomposition is $\pi = \pi_L + \pi_Q + \pi_\nu$, where the viscous part π_ν is harmonic and enforces (3). The present analysis ultimately concerns the wall-pressure contribution induced by π_Q, but the full statement is useful because it makes clear where the linear, nonlinear and viscous contributions enter.

For the nondimensional decomposition used below, lengths are normalised by the channel half-height h, velocities by the centreline velocity U_{cl}, and the kinematic pressure by U_{cl}^2, so that $Re = U_{cl} h/\nu$ and $y_w \in \{-1, 1\}$. Then

$$\partial_i \partial_i \pi_L = L, \qquad \left(\partial_y \pi_L\right)\big|_{y_w} = 0, \tag{4a}$$

$$\partial_i \partial_i \pi_Q = Q, \qquad \left(\partial_y \pi_Q\right)\big|_{y_w} = 0, \tag{4b}$$

$$\partial_i \partial_i \pi_\nu = 0, \qquad \left(\partial_y \pi_\nu\right)\big|_{y_w} = Re^{-1}\,\partial_y \partial_y v, \tag{4c}$$

where $\tilde{u}_i = U_i + u_i$, with $U(y)$ the mean streamwise velocity, $U_i = (U(y), 0, 0)$, and $u_i = (u, v, w)$. Here $L \equiv -2\,(\mathrm{d}U/\mathrm{d}y)\,\partial_x v$, $y_w \in \{-1, 1\}$ denotes the wall location, and Re is the Reynolds number used in the chosen nondimensionalisation. The boundary condition for π_ν in (4) is the nondimensional form of (3). The source terms analysed here are evaluated a posteriori from the stored velocity field of the $\delta^+ \approx 550$ incompressible channel DNS used in Huang *et al.* (2026) and Massey *et al.* (2025). No new simulation is introduced here.

The first exact representation (excluding the mean as discussed later) of the nonlinear source is the standard gradient-product form,

$$\begin{gathered} Q = -\partial_j \partial_k \left(u_j u_k\right) = -\partial_j u_k\,\partial_k u_j = \sum_{(ij)} Q_{ij}, \\ (ij) \in \{xx, yy, zz, xy, xz, yz\}, \end{gathered} \tag{5}$$

with

$$\begin{aligned} Q_{xx} &= -\left(\partial_x u\right)^2, & Q_{xy} &= -2\left(\partial_x v\right)\left(\partial_y u\right), \\ Q_{yy} &= -\left(\partial_y v\right)^2, & Q_{xz} &= -2\left(\partial_x w\right)\left(\partial_z u\right), \\ Q_{zz} &= -\left(\partial_z w\right)^2, & Q_{yz} &= -2\left(\partial_y w\right)\left(\partial_z v\right). \end{aligned} \tag{6}$$

This form is convenient numerically, but its six terms are not elementary physical contributions. The off-diagonal terms already mix rotation and strain, so a modest value of Q_{xy}, Q_{xz}, or Q_{yz} can hide a much larger positive–negative balance.

Rewriting the fluctuating velocity-gradient tensor in terms of its symmetric and antisymmetric parts, following Bradshaw & Koh (1981), the full pressure Poisson equation may also be written as

$$\partial_i \partial_i \pi = \underbrace{2\Omega_z \partial_x v}_{L} + \underbrace{\left(\overbrace{\tfrac{1}{2}\omega_i \omega_i}^{T} - \overbrace{S_{ij} S_{ij}}^{S}\right)}_{Q}, \tag{7}$$

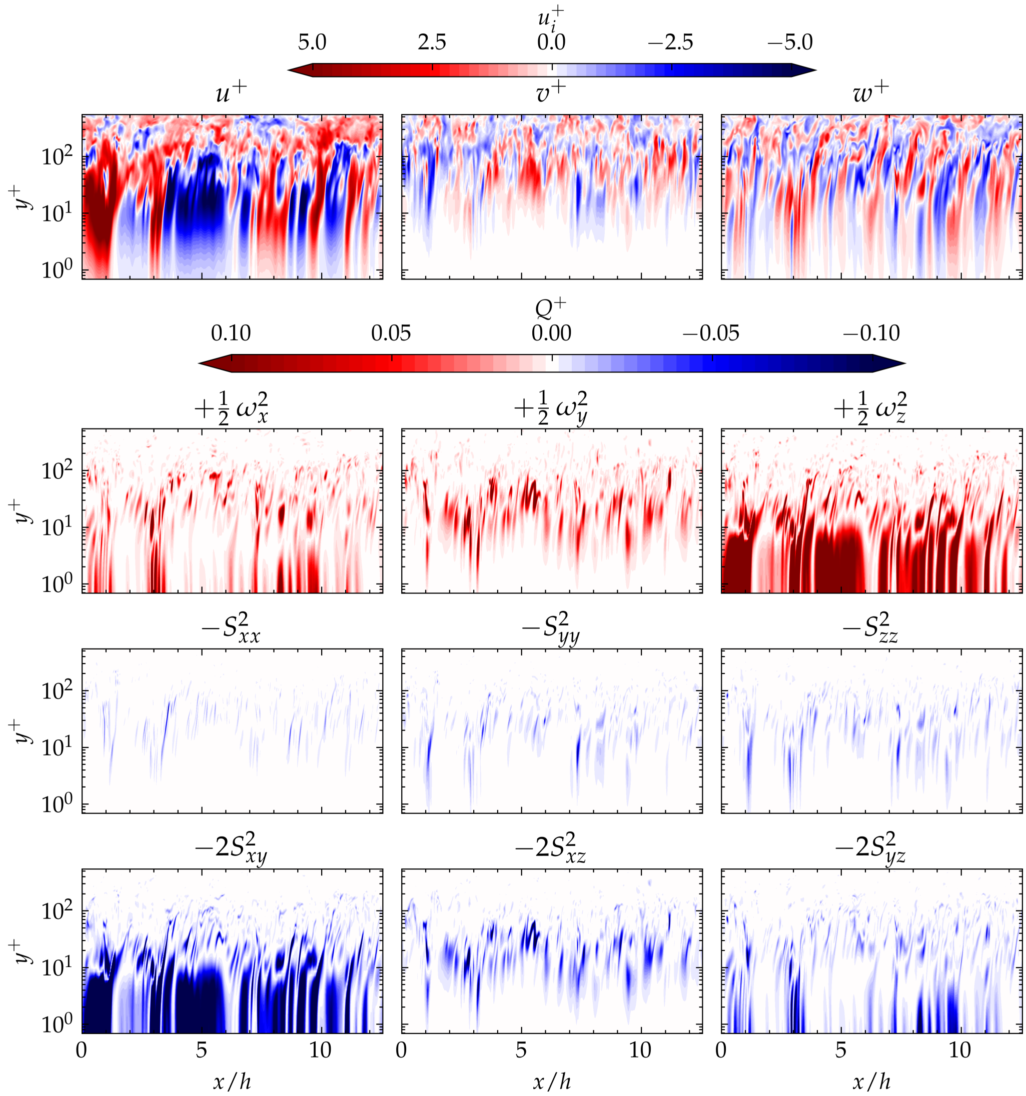

Figure 2. Instantaneous fields of the three velocity components and the nine vorticity/strain contributions to the nonlinear source term Q in an x–y plane from the $\delta^+ \approx 550$ DNS. The strongest near-wall sheets of $(+\frac{1}{2}\omega_z^2, -2S_{xy}^2)$ are consistent with sharp streamwise-velocity jumps across wall-attached interfaces, while $(+\frac{1}{2}\omega_y^2, -2S_{xz}^2)$ and $(+\frac{1}{2}\omega_x^2, -2S_{yz}^2)$ extend more broadly through the buffer/inertial layer.

Here L, T, and S denote the linear, enstrophy, and strain contributions, respectively; the required kinematic quantities are

$$\Omega_z = -\frac{\mathrm{d}U}{\mathrm{d}y}, \qquad \omega_i = \varepsilon_{ijk}\partial_j u_k, \qquad S_{ij} = \tfrac{1}{2}\left(\partial_i u_j + \partial_j u_i\right). \tag{8}$$

where ε_{ijk} is the Levi-Civita symbol.

Restricting attention to the nonlinear source gives

$$\begin{aligned} Q = \tfrac{1}{2}\,\omega_x^2 + \tfrac{1}{2}\,\omega_y^2 + \tfrac{1}{2}\,\omega_z^2 \\ -S_{xx}^2 - S_{yy}^2 - S_{zz}^2 \\ -2\,S_{xy}^2 - 2\,S_{xz}^2 - 2\,S_{yz}^2, \end{aligned} \tag{9}$$

where $Q = \sum_{m\in M} Q_m$, m indexes the nine vorticity/strain constituents, and $M = \{\omega_x, \omega_y, \omega_z, S_{xx}, S_{yy}, S_{zz}, S_{xy}, S_{xz}, S_{yz}\}$. The bridge between the two forms is especially revealing for the off-diagonal terms,

$$\begin{aligned} Q_{xy} &= \tfrac{1}{2}\,\omega_z^2 - 2\,S_{xy}^2, \\ Q_{xz} &= \tfrac{1}{2}\,\omega_y^2 - 2\,S_{xz}^2, \\ Q_{yz} &= \tfrac{1}{2}\,\omega_x^2 - 2\,S_{yz}^2, \end{aligned} \tag{10}$$

These identities also admit a direct kinematic interpretation: the positive $\frac{1}{2}\omega_i^2$ terms quantify local rotational intensity, whereas the negative $2S_{ij}^2$ terms quantify the corresponding strain intensity. Each off-diagonal Q_{ij} therefore represents, in the pressure source, the local imbalance between rotational and straining motions. By contrast, $Q_{xx} = -S_{xx}^2$, $Q_{yy} = -S_{yy}^2$, and $Q_{zz} = -S_{zz}^2$ are purely strain contributions. It is therefore useful to regard Q_{xy}, Q_{xz}, and Q_{yz} as residuals,

$$R_{xy} \equiv Q_{xy}, \qquad R_{xz} \equiv Q_{xz}, \qquad R_{yz} \equiv Q_{yz}, \tag{11}$$

with R_{xy}, R_{xz}, and R_{yz} arising from the three cancellations in (10). A small value of Q_{xy}, for example, does not imply that spanwise vorticity is dynamically unimportant; it may instead reflect a tight cancellation between $+\frac{1}{2}\omega_z^2$ and $-2S_{xy}^2$. This is precisely the ambiguity that the vorticity/strain form removes.

In the numerical implementation, $\partial_y u$ is formed from the fluctuating streamwise velocity by removing the wall-parallel zero mode $k = \mathbf{0}$, equivalently the instantaneous plane mean $\langle u \rangle_{xz}(y,t)$, before taking gradients. This ensures that ω_z and S_{xy} are constructed from fluctuating gradients only, so that the mean shear is not folded back into the nonlinear source representation.

Figure 2 shows snapshots of the three velocity components and the nine vorticity/strain fields from the $\delta^+ \approx 550$ DNS. The structural correspondence between the velocity fields and the source components is immediate. This qualitative agreement supports the use of streamwise velocity–pressure correlations as indicators of regions with strong Poisson-source activity (Gibeau & Ghaemi, 2021; Deshpande *et al.*, 2025). In particular, the strong velocity–pressure correlation reported by Deshpande *et al.* (2025) is consistent with the UMZ/fissure picture of Massey *et al.* (2025). Of the three off-diagonal balances, $(+\frac{1}{2}\omega_z^2, -2S_{xy}^2)$ is the most intense closest to the wall and reaches deepest toward it, whereas $(+\frac{1}{2}\omega_x^2, -2S_{yz}^2)$ forms broader tilted structures farther from the wall, some extending toward it, and $(+\frac{1}{2}\omega_y^2, -2S_{xz}^2)$ remains concentrated in the buffer/inertial layer. The diagonal strain terms are quantitatively weaker. This spatial organisation foreshadows the source-density balance.

The nonlinear pressure contributions are obtained from an integral convolution with the channel Green's-function kernel. Here we consider only the bottom wall ($y/h = -1$), so the bottom-wall superscript is dropped on pressure quantities. For the total nonlinear source and for each constituent Q_m, the wall-pressure Fourier amplitudes are

$$\begin{gathered}\widehat{p}_Q(k) = \int_{-1}^{1} G^-(k,y')\,\widehat{Q}(y',k)\,\mathrm{d}y', \\ \widehat{p}_{Q_m}(k) = \int_{-1}^{1} G^-(k,y')\,\widehat{Q}_m(y',k)\,\mathrm{d}y', \\ k = (k_x,k_z), \qquad k = |k| > 0,\end{gathered} \tag{12}$$

where $k = (k_x,k_z)$ is the wall-parallel wavenumber vector, $k = |k|$ its magnitude, and y' denotes the wall-normal source coordinate, so the wall-pressure contribution from a source layer at y' depends both on its local intensity and on the elliptic weight G^-. Here $G^-(k,y')$, with y' denoting a generic wall-normal source location, is the standard Green's-function kernel for the channel-flow bottom wall (Kim, 1989); writing it in exponential form makes the wall-normal attenuation explicit:

$$G^-(k,y') = -\frac{1}{k}\,\frac{\mathrm{e}^{-k(1+y')} + \mathrm{e}^{-k(3-y')}}{1-\mathrm{e}^{-4k}} \;\xrightarrow[k\gg 1]{}\; -\frac{1}{k}\mathrm{e}^{-k(1+y')}, \tag{13}$$

Because the Poisson solve is linear, the pressure decomposition is additive,

$$\widehat{p}_Q = \sum_{m\in M} \widehat{p}_{Q_m}. \tag{14}$$

In practice, only the non-zero wall-parallel Fourier modes are retained in the wall-pressure reconstruction, so the $k = \mathbf{0}$ mode of Q—the component constant in both x and z, equivalently the instantaneous plane mean $\langle Q \rangle_{xz}(y,t)$—does not contribute. The kernel decays approximately exponentially away from the wall over a scale $O(1/k)$, so short wavelengths are supplied predominantly by near-wall motions, whereas long wavelengths sample sources farther from the wall (Massey *et al.*, 2025).

SOURCE-DENSITY ATTRIBUTION OF THE Q TERMS

Like Anantharamu & Mahesh (2020), we use a Green's-function-based source-attribution framework. Unlike their frequency-resolved plane-pair analysis, however, the present approach collapses the wall-parallel correlations into a one-point wall-normal source density for wall-pressure variance and applies it term-by-term to compare exact decompositions of the nonlinear source. Application of the source-density construction to (12)–(14) gives

$$\langle p_Q^2 \rangle = \int_{-1}^{1} S_Q(y)\,\mathrm{d}y, \tag{15}$$

with

$$\begin{gathered}S_Q(y) = \sum_{k\neq\mathbf{0}} \Re\left\{ G^-(k,y)\,\left\langle \widehat{Q}(y,k)\,\widehat{p}_Q^*(k) \right\rangle \right\}, \\ \widehat{Q} = \sum_{m\in M} \widehat{Q}_m.\end{gathered} \tag{16}$$

The exact attributed contribution of each individual term is then defined by

$$\langle p_{Q_m} p_Q \rangle = \int_{-1}^{1} S_{Q_m}(y)\,\mathrm{d}y, \tag{17}$$

with

$$S_{Q_m}(y) = \sum_{k\neq\mathbf{0}} \Re\left\{ G^-(k,y)\,\left\langle \widehat{Q}_m(y,k)\,\widehat{p}_Q^*(k) \right\rangle \right\}. \tag{18}$$

This construction preserves exact additivity,

$$S_Q(y) = \sum_{m\in M} S_{Q_m}(y), \qquad \langle p_Q^2 \rangle = \sum_{m\in M} \langle p_{Q_m} p_Q \rangle. \tag{19}$$

In plus units, the cumulative contribution accrued with increasing wall-normal distance from the wall, up to a cutoff y_c^+, is

$$\begin{gathered}C_{Q_m}(y_c^+) = \int_0^{y_c^+} S_{Q_m}^+(y'^+)\,\mathrm{d}y'^+, \\ C_Q(y_c^+) = \sum_{m\in M} C_{Q_m}(y_c^+).\end{gathered} \tag{20}$$

Figure 3(a) shows that the gradient-product view is dominated by Q_{xz} and Q_{yz}, both of which make positive contributions that peak in the buffer/inertial layer. The Q_{xz} contribution is broader and remains positive over a larger wall-normal range, whereas Q_{yz} is more localised. The largest negative corrections come from Q_{yy} and Q_{zz}, while Q_{xx} and Q_{xy} are comparatively small. Read in isolation, this representation suggests that Q_{xy} plays only a minor role.

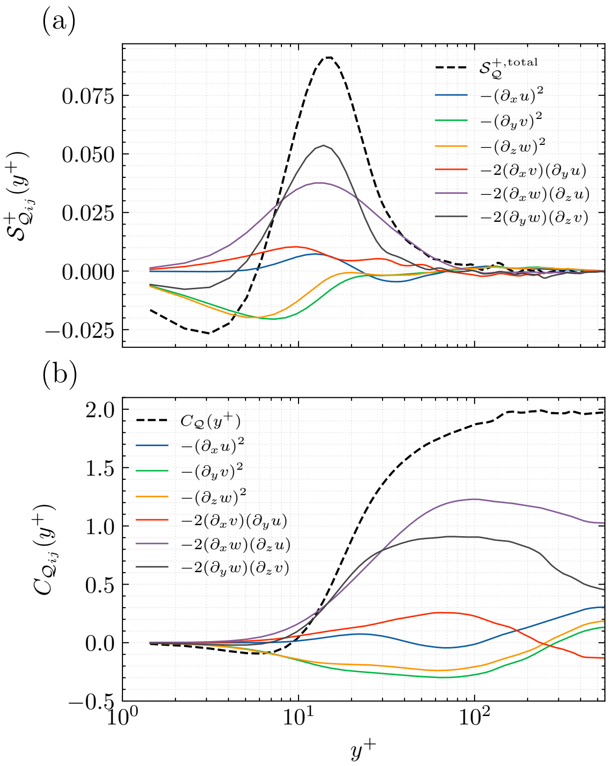

Figure 3. Source-density attribution of the six gradient-product terms in Q. (a) $S^{+}_{Q_{ij}}(y^{+})$. (b) $C_{Q_{ij}}(y^{+})$. The dashed line denotes the total nonlinear contribution.

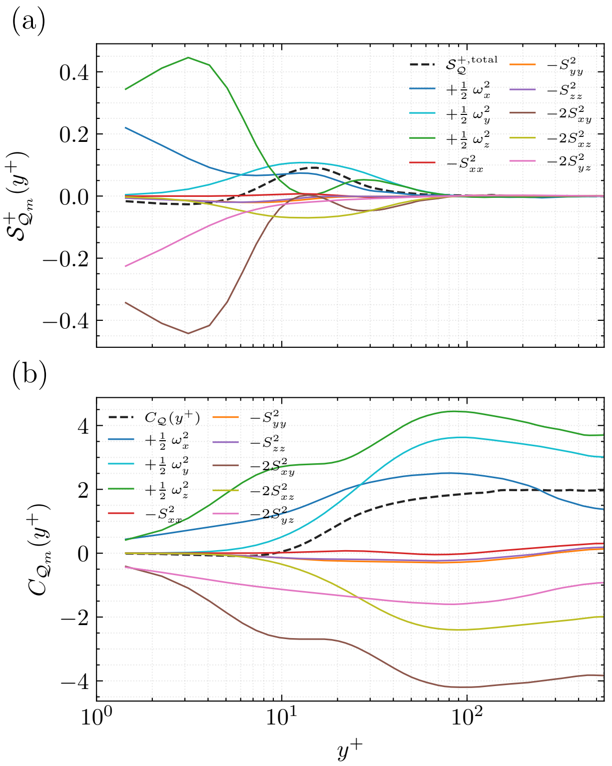

Figure 4. Source-density attribution of the nine vorticity/strain terms in Q. (a) $S^{+}_{Q_m}(y^{+})$. (b) $C_{Q_m}(y^{+})$. The dashed line denotes the total nonlinear contribution.

The vorticity/strain view in figure 4 makes clear why that conclusion is misleading. The weak net contribution of Q_{xy} reflects one of the tightest cancellations in the problem: $+\frac{1}{2}\omega_z^2$ and $-2S_{xy}^2$ are individually among the largest near-wall source terms, but their difference is modest after wall attribution. Figure 4 (a) shows that the total nonlinear source density is assembled from three dominant pairwise balances. Very near the wall, $+\frac{1}{2}\omega_z^2$ and $-2S_{xy}^2$ reach the largest magnitudes, both of order 0.45 in $S^{+}_{Q_m}$, but nearly cancel. Across roughly $10 \lesssim y^+ \lesssim 60$, the broader pairs $(+\frac{1}{2}\omega_y^2, -2S_{xz}^2)$ and $(+\frac{1}{2}\omega_x^2, -2S_{yz}^2)$ supply the positive peak in the total S^{+}_{Q}, which occurs at $y^+ = O(12)$. The diagonal strain terms $-S_{xx}^2$, $-S_{yy}^2$, and $-S_{zz}^2$ remain much smaller throughout.

Figure 4 (b) quantifies the imbalance. By $y^+ \sim 10^2$, the cumulative positive contributions from $+\frac{1}{2}\omega_z^2$, $+\frac{1}{2}\omega_y^2$, and $+\frac{1}{2}\omega_x^2$ are each of order 2.5, 3.5, and 4.5. These are offset primarily by $-2S_{xy}^2$, $-2S_{xz}^2$, and $-2S_{yz}^2$, whose cumulative corrections are approximately order -4, -2.5, and -1.5, respectively, while the diagonal strain terms contribute only small negative corrections. The total nonlinear contribution, $C_Q \approx 2$, is therefore the small positive remainder of much larger positive and negative terms.

The reason figure 4 is more revealing than figure 3 is that the positive enstrophy and negative strain pieces in (10) are plotted separately. If one could decompose the off-diagonal gradient-product terms into comparably additive signed pieces, the same cancellations would of course reappear. The difficulty is that, for example, $Q_{xy} = -2(\partial_x v)(\partial_y u)$ contains its two velocity gradients only multiplicatively, so there is no unique additive attribution of the wall-pressure source to one factor or the other while preserving exact closure of Q. By contrast, the decomposition in (9) and (10) is exact, additive, and separates the competing positive and negative contributors. That is why the vorticity/strain form identifies the physically relevant cancellations, whereas the gradient-product form reports only their residuals.

RESULTS & CONSEQUENCES

The principal result here is not a Reynolds-number scaling law, but a mechanism. In a channel flow at $\delta^+ \approx 550$, the nonlinear wall-pressure source seems to be most clearly interpreted in the exact vorticity/strain form rather than in the standard gradient-product form. The latter packages the dynamics into six mixed quantities, three of which are already residuals of large positive and negative contributions. The former reveals that the source is assembled from three dominant cancellations:

$$
\begin{aligned}
&+\tfrac{1}{2}\omega_z^2 \leftrightarrow -2S_{xy}^2,\\
&+\tfrac{1}{2}\omega_y^2 \leftrightarrow -2S_{xz}^2,\\
&+\tfrac{1}{2}\omega_x^2 \leftrightarrow -2S_{yz}^2.
\end{aligned}
\tag{21}
$$

The first pair is strongest closest to the wall, while the latter two provide the broader buffer/inertial-layer support. The total source-density peak is the positive remainder of these incomplete cancellations, not the signature of a single isolated source term. In every dominant pair, the vorticity contribution exceeds the corresponding strain contribution in net, so the nonlinear source is enstrophy-dominated after wall attribution.

This algebraic result is consistent with the structural picture in figure 1. The dominant positive pieces are carried by thin vortical-fissure-like interfaces separating neighbouring momentum zones, while the compensating negative strain terms arise in the same interfaces. Near the wall, the strongest such interface gives the intense $(+\frac{1}{2}\omega_z^2, -2S_{xy}^2)$ balance. Farther from the wall, tilted and stretched interfaces supply the broader $(+\frac{1}{2}\omega_y^2, -2S_{xz}^2)$ and $(+\frac{1}{2}\omega_x^2, -2S_{yz}^2)$ balances. The latter is naturally interpreted as the signature of cross-plane roll motions associated with streamwise-oriented vortical structures: around the flanks of lifted low-speed streaks, or equivalently warped momentum-zone interfaces, counter-rotating motion in the y–z plane generates streamwise vorticity ω_x, while the same wall-normal/spanwise velocity gradients generate the companion strain S_{yz}. The wall-pressure source is therefore not tied to one isolated constituent, but to the small residual left after those sheetlike vortical/strain structures are mapped elliptically to the wall.

This reinterpretation sharpens the modelling target. A reduced experimental surrogate or numerical closure need not reproduce each component of the gradient-product representation separately; it must instead preserve the relative strength of the three balances in (21) and the small residual that survives them. Matching the total Q field while misrepresenting those cancellations would still give the wrong wall-pressure source.

The present paper does not establish the Reynolds-number scaling of the individual pair residuals. It identifies, at one representative δ^+, the balance whose scaling should be tested next in multi-δ^+ datasets and across other canonical wall flows. That is the natural next step if one wishes to connect the known logarithmic growth of $\langle p^{+2} \rangle$ to a reduced, experimentally accessible description of the nonlinear source.

ACKNOWLEDGEMENTS

The support from DARPA under award # HR0011-24-9-0465 and the support of ONR to CTR under grant # N000142312833 is gratefully acknowledged.

REFERENCES

Anantharamu, Sreevatsa & Mahesh, Krishnan 2020 Analysis of wall-pressure fluctuation sources from direct numerical simulation of turbulent channel flow. *J. Fluid Mech.* **898**, A17.

Bautista, Juan Carlos Cuevas, Ebadi, Alireza, White, Christopher M., Chini, Gregory P. & Klewicki, Joseph C. 2019 A uniform momentum zone-vortical fissure model of the turbulent boundary layer. *J. Fluid Mech.* **858**, 609–633.

Bradshaw, P. & Koh, Y. M. 1981 A note on Poisson's equation for pressure in a turbulent flow. *The Physics of Fluids* **24** (4), 777.

Dacome, Giulio, Lazzarini, Lorenzo, Talamelli, Alessandro, Bellani, Gabriele & Baars, Woutijn J. 2025 Scaling of wall-pressure-velocity correlations in high-Reynolds-number turbulent pipe flow. *J. Fluid Mech.* **1013**, A48.

Deshpande, Rahul, Hassanein, Abdelrahman & Baars, Woutijn J. 2025 Source locations and convection velocities of outer-scaled wall-pressure fluctuations in canonical turbulent boundary layers. *arXiv:2508.19940* .

Fritsch, Danny, Vishwanathan, Vidya, Duetsch-Patel, Julie, Gargiulo, Aldo, Lowe, Kevin T & Devenport, William J 2020 The pressure signature of high Reynolds number smooth wall turbulent boundary layers in pressure gradient family. In *AIAA Aviation 2020 Forum*, p. 3066.

Gibeau, Bradley & Ghaemi, Sina 2021 Low- and mid-frequency wall-pressure sources in a turbulent boundary layer. *J. Fluid Mech.* **918**, A18.

Huang, Yuting, Toedtli, Simon S., Chini, Gregory P. & McKeon, Beverley J. 2026 Spatio-temporal characterization of nonlinear forcing and response in turbulent channel flow. *J. Fluid Mech. (to appear)* .

Kim, John 1989 On the structure of pressure fluctuations in simulated turbulent channel flow. *J. Fluid Mech.* **205**, 421.

Klewicki, J. C., Priyadarshana, P. J. A. & Metzger, M. M. 2008 Statistical structure of the fluctuating wall pressure and its in-plane gradients at high Reynolds number. *J. Fluid Mech.* **609**, 195–220.

Mansour, N. N., Kim, J. & Moin, P. 1988 Reynolds-stress and dissipation-rate budgets in a turbulent channel flow. *J. Fluid Mech.* **194**, 15–44.

Massey, Jonathan M. O., Klewicki, Joseph C. & McKeon, Beverley J. 2025 Behind the logarithmic growth of inner-scaled wall-pressure variance. *arXiv:2511.16776* .

Massey, Jonathan M. O., Smits, Alexander J. & McKeon, Beverley J. 2026 Eddy population based model for the wall-pressure spectrum at high Reynolds number. *J. Fluid Mech. (accepted)* .